



Development of composite ultrafiltration membrane made of PmPD/PVA layer deposited on ceramic pozzolan/micronized phosphate support and its application for Congo red dye removal

D. Beqqour^{a,*}, G. Derouich^a, W. Taanaoui^a, A. Essate^a, M. Ouammou^a, S. Alami Younssi^a, J. Bennazha^a, J.A. Cody^b, M. El Rhazi^a

^aLaboratory of Materials, Membranes, and Environment, Faculty of Sciences and Technologies Mohammedia, University Hassan II of Casablanca, Casablanca, Morocco, emails: dounia.beqqour-etu@etu.univh2c.ma (D. Beqqour), gh.derouich@gmail.com (G. Derouich), wiametaanaoui@gmail.com (W. Taanaoui), ahlam.essate@gmail.com (A. Essate), mouammou@yahoo.fr (M. Ouammou), alamiyounssisaad@yahoo.fr (S.A. Younssi), jbenazha@yahoo.fr (J. Bennazha), elrhazim@hotmail.com (M. El Rhazi)

^bDepartment of Chemistry, Lake Forest College, 555 N. Sheridan Rd., Lake Forest, IL, USA, email: cody@mx.lakeforest.edu

Received 2 March 2021; Accepted 21 May 2021

ABSTRACT

This work aims to develop a new composite ultrafiltration membrane (CM) by deposition of poly(m-phenylenediamine) and poly(vinyl alcohol) on flat porous support made from pozzolan and micronized phosphate. The poly(m-phenylenediamine) was synthesized by chemical polymerization of m-phenylenediamine and added to poly(vinyl alcohol) in order to prepare the suspension. The selective layer was deposited on the flat support via dip-coating with different poly(vinyl alcohol) content, ranging from 8 to 12 wt.%, and kept for 24 h under 60°C. The obtained CM was characterized by Fourier transform infrared spectroscopy, water contact angle, permeability, scanning electron microscopy, energy dispersive X-ray analysis, and filtration performances. The optimized membrane containing 10 wt.% of poly(vinyl alcohol) is homogenous and exhibits a good adhesion on the pozzolan/micronized phosphate support. Furthermore, the CM has a water contact angle of about 80°, a permeability of 203.66 L/h m² bar a thickness of 19.67 μm, and a pore size of 71 nm. In addition, the filtration performance of the membrane was evaluated by filtration of Congo red dye. The effect of operating pressure (1–3 bar), feed concentration (20–600 ppm), and feed pH (4–10) were investigated. The CM was able to remove up to 98.63% of Congo red under optimal conditions ($\Delta P = 3$ bar, $C = 600$, and $\text{pH} = 4$).

Keywords: Composite membrane; Poly(m-phenylenediamine); Poly(vinyl alcohol); Pozzolan/micronized phosphate; Congo red dye; Ultrafiltration

1. Introduction

Water is the most precious, essential resource on the planet for any living organism [1]. In recent decades, the excessive consumption of water resources due to the industrial revolution, agricultural development, and population growth affect its worldwide availability [2]. Therefore, a significant amount of wastewater is discharged [3] particularly from pharmaceutical [4], cosmetic [5], and paper industries [6] as well as textile effluents [7].

Production processes in different industrial fields depend on chemical products, heavy metals, and organic materials including synthetic dyes that end up in wastewater streams and must be treated before release. In particular, aqueous solutions of synthetic dyes that are chemically/thermally stable and non-biodegradable can directly damage both the environment and human health [8].

In this regard, the treatment and the reuse of wastewater have become an obligation to alleviate water scarcity [9]. Several physico-chemical and biological techniques have been used for the removal of dyes including: adsorption

* Corresponding author.

Presented at the Second International Symposium on Nanomaterials and Membrane Science for Water, Energy and Environment (SNMS-2021), June 1–2, 2022, Tangier, Morocco

by conventional (activated carbon) [10] or unconventional adsorbents (pozzolan) [11], electrochemical methods [12], ion exchange [13], coagulation–floculation [14], and encapsulation processes [15]. Among wastewater treatment techniques, membrane filtration, particularly low-pressure ultrafiltration (UF) may remain the best choice for dye removal owing to its selectivity, efficiency, and economic reliability [16,17].

UF membranes can be fabricated with different materials. Depending on the nature of the material used, three types of membranes are possible: polymeric (organic material), ceramic (mineral material), and composite membrane (CM) where more than one material is required [18]. Generally, the organic membranes are made from cellulose, polysulfone, and polyamide [19–21]. This type of membrane is frequently used due to its low cost but it has drawbacks such as low mechanical, chemical, and thermal resistance as well as a short lifetime. In contrast, ceramic membranes are usually more costly than polymeric ones. This can be related to the use of expensive raw materials such as alumina, zirconia, and titania as well as manufacturing complexity. However, they present a high resistance (mechanically, chemically, and thermally) and have long-term durability [18].

In recent years, the development of thin-film CMs has attracted much attention through several studies that combine the qualities of polymeric and ceramic membranes, leading to a strong, and selective CM. For instance, Derouich et al. [22] have developed a new CM using flat ceramic support based on pozzolan and a thin film of polypyrrole for the removal of the anionic congo red dye (CR). Similarly, Benkhaya et al. [23] used flat pozzolan support with a polysulfone layer for CMs capable of filtering dyes including acid orange 74 and methyl orange [23]. Another study used tubular ceramic support to prepare a CM with PVA for the production of bio-ethanol [24].

The present work aims to develop a new CM using poly(m-phenylenediamine) (PmPD) and poly(vinyl alcohol) (PVA) as a thin film deposited on flat microfiltration (MF) pozzolan membrane incorporated with micronized phosphate (Pz/MP) that was developed in our previous study [25]. This MF membrane that will be used as support was selected owing to its appropriate characteristics: good porosity (32.07%), permeability (1,732.50 L/h m² bar), and high mechanical resistance. Additionally, it was prepared from environmentally friendly and abundant geomaterials.

PmPD and PVA polymers were selected as the active layer because PmPD is insoluble in any organic solvent under neutral conditions and it easily aggregates in water, thus promoting layer formation [26]. In addition, the m-phenylenediamine (mPD) exhibits a high oxidative polymerization yield. For this purpose, the fine, nontoxic, and odor-free microparticles were prepared by a simple oxidative precipitation polymerization from mPD [27].

PVA is an environmentally friendly polymer, with low-cost, and wide use in the manufacture of UF membranes due to its excellent mechanical properties, chemical and thermal resistance, hydrophilicity, and water permeability [28,29], anti-fouling, and film-forming propensity [30,31]. Consequently, all these specific properties of PVA will allow the preparation of a chemically, thermally, and

mechanically resistant membrane with a thin homogeneous layer that is also resistant to fouling. Furthermore, the dense network structure of the PVA will embed and constrain PmPD into the network [26].

In order to ensure the formation of PmPD and to examine the surface characteristics of the developed PmPD/PVA membrane, samples were characterized by Fourier transform infrared spectroscopy (FTIR), scanning electron microscopy (SEM), energy dispersive X-ray analysis (EDX), pore size, and water contact angle (WCA) measurements. The optimized PmPD/PVA membrane was selected based on the performance metrics obtained by varying the PVA content in the deposit solution.

This membrane was evaluated by studying the parameters influencing CR dye rejection namely operating pressure, feed concentration, and feed pH using cross-flow filtration.

2. Experimental

2.1. Materials

The flat Pz/MP ceramic support was used for the preparation of the CM as described elsewhere [25]. The main characteristics of the support are reported in Table 1. PVA (Rhodoviol 25/140) and ferric chloride hexahydrate LR (FeCl₃, 98%) were purchased from Prolabo and SDFCL, respectively. Both mPD monomer and CR dye (35%) were obtained from Sigma Aldrich.

CR is a sodium salt of benzidine diazo-bis-1-naphthyl-amino-4-sulfonic acid. Additional characteristics of this dye are shown in Table 2. All water used in this work was distilled prior to use.

2.2. Chemical polymerization of the mPD

To the mPD monomer (1 M), the oxidant FeCl₃ (4 M) was added dropwise with constant stirring and it was left stirring for 6 h to complete the polymerization. The formed polymer was collected by filtration and washed several times with distilled water then was dried.

2.3. Preparation of the PmPD/PVA membrane

In the first step, the Pz/MP support was cleaned with water via ultrasound irradiation in order to eliminate any residual particles, then dried overnight at 100°C. In the second step, the same amount of PmPD was added to the PVA solution (8, 10, and 12 wt.% of PVA) with constant

Table 1
Characteristics of the flat Pz/MP support

| | |
|---|----------|
| Diameter (mm) | 37 |
| Thickness (mm) | 2.90 |
| Shrinkage (%) | 1.80 |
| Porosity (%) | 32.07 |
| Pore size (μm) | 1.33 |
| Water permeability (L/h m ² bar) | 1,732.50 |
| Mechanical strength (MPa) | 15.69 |

magnetic stirring. The mass ratio of PmPD/PVA is equal to 0.57, 0.45, and 0.36 for membrane with 8, 10, and 12 wt.% of PVA, respectively.

The Pz/MP support was coated using the PmPD/PVA suspension by dip-coating in atmospheric conditions. Thereafter, the membrane was kept in air for 1 h, then dried for 24 h at 60°C before evaluation, and characterization.

2.4. UF experiments

The cross-flow filtration experiment was carried out using a stainless steel UF pilot described in Fig. 1. It is composed of a feed tank of 5 L, circulation pump, membrane housing with 4.52 cm² of filtering surface area, manometers, and an air compressor. The cooling system was used to maintain a constant temperature during the experiments. Water permeability for all the studied membranes was determined from filtration of water under different pressures ranging from 1 to 3 bar at room temperature.

The permeate flux J_w (L/h m²) and the permeability L_p (L/hm²bar) were calculated using Eqs. (1) and (2), respectively:

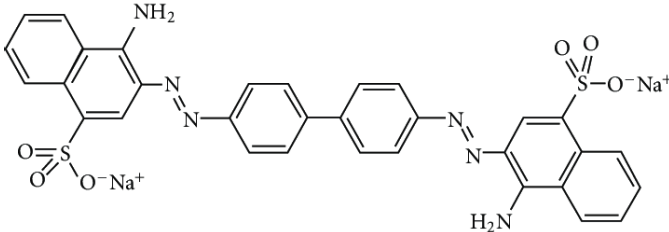
$$J_w = \frac{V}{A \cdot t} \quad (1)$$

$$L_p = \frac{J_w}{\Delta P} \quad (2)$$

where V (L) is the volume of permeate collected during the time interval t (h), A is the effective membrane area (m²), and ΔP is the operating pressure (bar).

The experimental parameters influencing filtration performance were studied using the optimized membrane. First, the effect of operating pressure was studied by varying the pressure from 1 to 3 bar. Second, the effect of feed concentration on membrane performance was investigated from 20 to 600 ppm. Finally, the feed pH was varied from 4

Table 2
Characteristics of CR dye

| | |
|--------------------------|--|
| Chemical formula | C ₃₂ H ₂₂ N ₆ Na ₂ O ₆ S ₂ |
| Molecular weight (g/mol) | 696.66 |
| Type of dye | Anionic |
| Chemical structure |  |

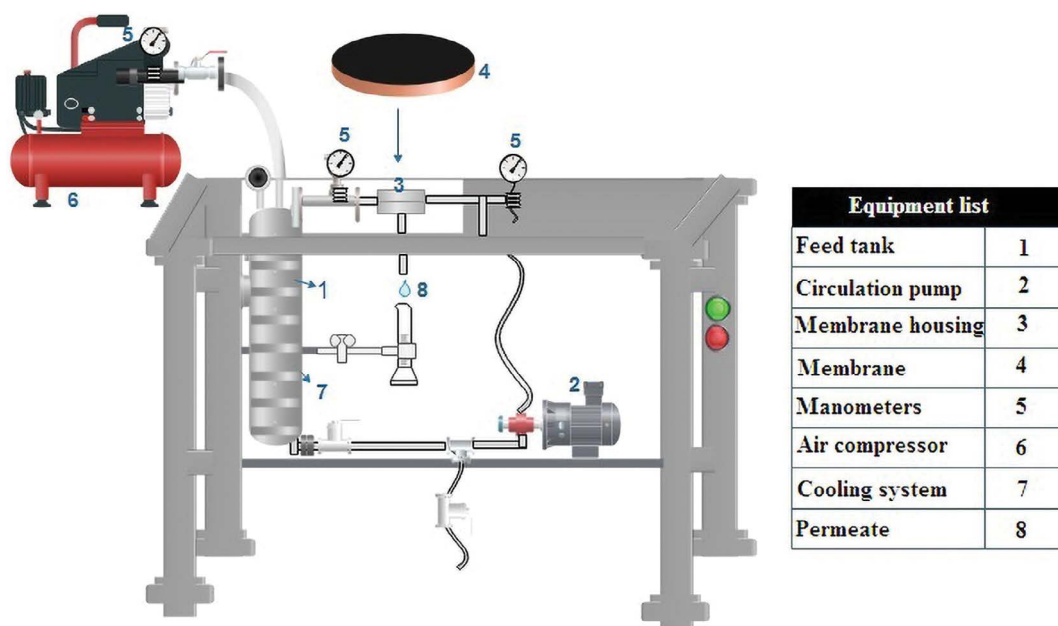


Fig. 1. Scheme of UF filtration pilot.

to 10 by adding drops of HCl (2 M) and NaOH (2 M) solutions. All the effects were studied over 2 h of filtration.

The rejection factor R (%) was calculated according to the following equation (Eq. (3)):

$$R = \left(1 - \frac{C_{\text{permeate}}}{C_{\text{feed}}} \right) \times 100 \quad (3)$$

where C_{permeate} and C_{feed} (ppm) are respectively the concentration of the permeate and the feed.

2.5. Antifouling study

The antifouling characteristics of the optimized membrane were evaluated under a pressure of 3 bar for 2 h. Several antifouling parameters namely flux recovery ratio (FRR), total flux decline ratio (TFR), reversible flux decline ratio (RFR), and irreversible flux decline ratio (IFR) could be calculated according to the following equations (Eqs. (4)–(7)) [32]:

$$\text{FRR} = \frac{J_{w1}}{J_{w0}} \times 100 \quad (4)$$

$$\text{TFR} = \left(1 - \frac{J_p}{J_{w0}} \right) \times 100 \quad (5)$$

$$\text{RFR} = \frac{J_{w1} - J_p}{J_{w0}} \times 100 \quad (6)$$

$$\text{IFR} = \frac{J_{w0} - J_{w1}}{J_{w0}} \times 100 \quad (7)$$

where J_{w0} is the water permeate flux of the membrane, J_p is the permeate flux of the membrane using CR dye at a concentration of 600 ppm. J_{w1} is the water permeate flux of the membrane measured for 2 h at 3 bar after physical cleaning and rising the membrane for 1 h using the UF pilot (pressure of 3 bar).

2.6. Characterization

FTIR analysis of the synthesized polymer, PVA, and the membrane layer (PmPD/PVA, peeled off of the ceramic support) was carried out using a Bruker spectrometer (Vertex 70). The morphology of the elaborated membranes was observed using an SEM operating at 10 kV (FEI Company, Quanta 200). An EDX detector on the SEM was used to identify the elemental composition of the optimized membrane.

The average pore size was calculated using the extended Hagen–Poisseuille equation (Eq. (8)) [33]:

$$d = 2 \sqrt{8J_w \cdot \delta \cdot \frac{\tau}{\epsilon} \cdot \frac{\Delta X}{\Delta P}} \quad (8)$$

where d (m) is the pore diameter, J_w (m/s) is the water flux, δ (Pa.s) is the water viscosity, τ is the tortuosity factor (2.5 for sphere particle packing), ϵ (%) is the porosity of the membrane, ΔP (Pa) is the applied pressure, and ΔX (m) is the membrane thickness.

In order to measure the hydrophilicity of the Pz/MP support and the elaborated CMs, the WCA was measured using a Digidrop goniometer (GBX Instruments).

The concentration of CR dye before and after filtration was measured by UV-vis spectrophotometry (JASCO V-730 spectrophotometer) using quartz cells at a wavelength of maximum absorbance of 499 nm. The pH was measured by a pH meter (METTLER TOLEDO SevenCompact pH/Ion).

The point of zero charge (PZC) of CM was determined by solid addition as described in other work [34].

3. Results and discussion

3.1. Membrane of PmPD/PVA characterization

3.1.1. FTIR analysis

The FTIR spectra of the PmPD, PVA, and PmPD/PVA layers are illustrated in Fig. 2. For the PmPD, the two peaks located at 3,320 and 3,200 cm^{-1} are attributed to the N–H stretching mode [26,35–37]. The peak at 1,620 cm^{-1} corresponds to the stretching mode of quinoid imine [38–40] and the peak at 1,508 cm^{-1} is ascribed to the stretching vibrations of benzenoid amine [41]. The peaks at 1,403 and 1,250 cm^{-1} are associated with the C–N stretching vibrations in benzenoid units [35,42,43]. The characteristic peaks at 1,105; 830; and 619 cm^{-1} together represent in-of-plane and out-of-plane bending vibrations of the C–H bonds of 1,2,4-trisubstituted benzene rings. This is consistent with a phenazine-like ladder structure involving both amino groups for PmPD [27,40,42,44]. All the above observations indicate the successful formation of PmPD.

The main peaks of PVA were observed at 3,280; 2,917; 1,718; 1,425; 1,324; 1,081; 916; and 839 cm^{-1} . The highest band intensity in the region of 3,280 cm^{-1} is associated with the O–H stretching vibration of the hydroxy group [45,46]. The peak located at 2,917 cm^{-1} is assigned to CH_2 asymmetric stretching vibration [46]. For the

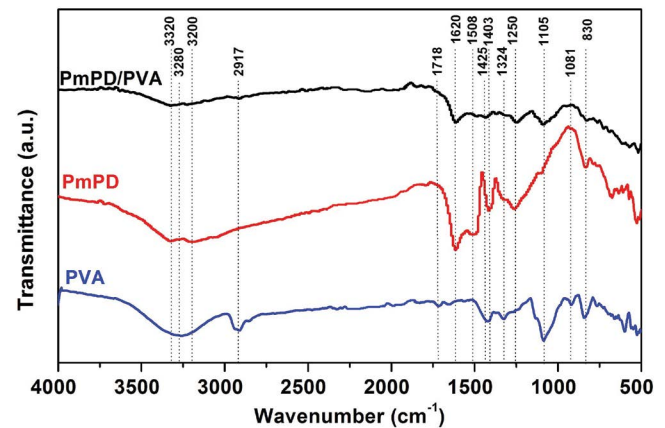


Fig. 2. FTIR spectra of PVA, PmPD, and PmPD/PVA membrane layer.

peak at $1,718\text{ cm}^{-1}$, it corresponds to the C=O vibration [26]. The peak at $1,425\text{ cm}^{-1}$ is due to C–H bending vibration of CH_2 [46] whereas the peak at $1,324\text{ cm}^{-1}$ is attributed to C–H deformation vibration [45]. The peak at $1,081\text{ cm}^{-1}$ is related to C–O stretching of acetyl groups [46]. The peak at 916 cm^{-1} is linked to CH_2 rocking [46], and the last peak at 839 cm^{-1} is due to C–C stretching [45].

From the spectrum corresponding to the PmPD/PVA membrane layer, there are some peaks that correspond to the PVA (peaks at $2,917$; $1,425$; and $1,081\text{ cm}^{-1}$) and others that correspond to the PmPD (peaks at $3,320$; $3,200$; $1,620$; $1,403$; and $1,250\text{ cm}^{-1}$). In addition, the peaks at 839 cm^{-1} from the PVA and 830 cm^{-1} from the PmPD overlap to form a new broad peak.

3.1.2. WCA measurement

The surface wettability technique was performed via WCA measurements of Pz/MP support and UF CMs in order to evaluate the influence of PVA content on membrane hydrophilicity. Fig. 3 shows results of WCA measurement of the support and CMs as a function of PVA content. The Pz/MP support has 21° of WCA which means that the support surface has a higher hydrophilic character. WCA value is about 77° , 80° , and 82° for membranes with 8, 10, and 12 wt.% of PVA, respectively. Increasing the PVA content slightly increases the WCA.

3.1.3. Permeability

The permeate flux of the membranes (8, 10, and 12 wt.%) as a function of operating pressure, which was varied from 1 to 3 bar, is depicted in Fig. 4. It is clear from Fig. 4 that the relationship is linear and therefore the permeability of the membranes could be calculated by determining the slope of these lines. The permeability of the membranes are $265\text{ L/h m}^2\text{ bar}$ for the membrane with 8 wt.% of PVA, $203.66\text{ L/h m}^2\text{ bar}$ for the membrane that contains 10 wt.% of PVA, and $170.35\text{ L/h m}^2\text{ bar}$ for the membrane with 12 wt.% of PVA. The permeability remarkably decreases when the amount of PVA increases. This drop-in permeability value could be explained by the fact that the membrane layer became thicker with the addition of PVA. This is consistent with SEM characterization (section SEM observation).

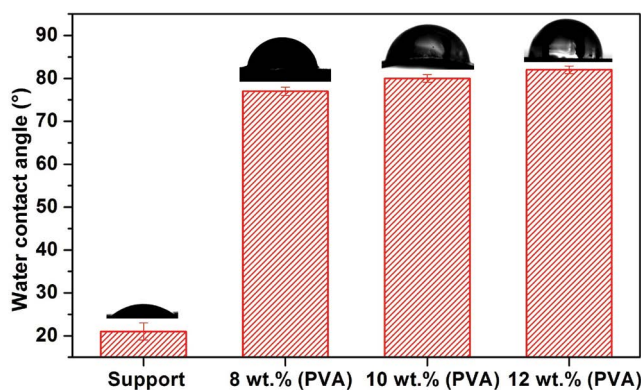


Fig. 3. WCA of Pz/MP support and PmPD/PVA membranes with different PVA content.

3.1.4. Pore size

Fig. 5 shows the pore size of prepared membranes. It can be clearly observed that the pore size of the membranes is 92, 71, and 62 nm when the PVA content is 8, 10, and 12 wt.%, respectively. This could be explained by the fact that the membrane layer becomes thicker with the addition of PVA content which leads to a reduction in the pore size in the membrane.

3.1.5. Membrane performance

Fig. 6 shows the permeate flux and the rejection of CR as a function of PVA content. Membrane performance in CR removal was evaluated by cross-flow filtration during 2 h with two concentrations: 20 and 100 ppm. The operating pressure was 3 bar. The permeate flux decreases when the amount of PVA increases from 8 to 12 wt.% as shown in Fig. 6a which is in agreement with the obtained values of the water permeability.

Rejection results of CR solution with concentrations of 20 and 100 ppm for the three membranes vs. wt.% PVA are presented in Fig. 6b. These results show that the rejection after 2 h of filtration is 88.22% (8 wt.% of PVA), 93.83% (10 wt.% of PVA), and 91.82% (12 wt.% of PVA) when the

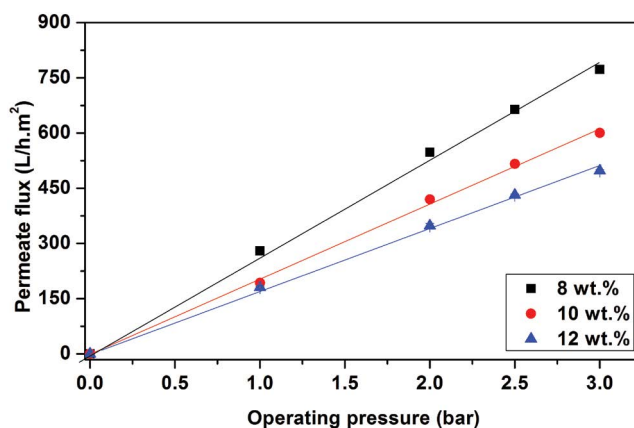


Fig. 4. Water permeate flux as a function of the operating pressure of CMs.

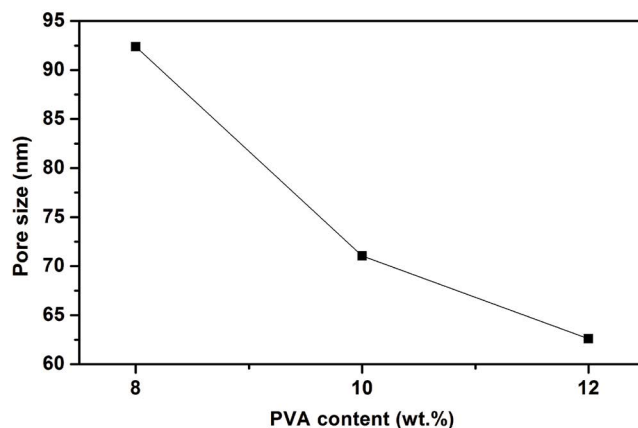


Fig. 5. Pore size of CMs with different PVA content.

feed concentration is 20 ppm. Increasing the feed concentration to 100 ppm, the rejection is about 49.54%, 94.01%, and 88.98% for membranes with 8, 10, and 12 wt.% of PVA content, respectively. These results are in accordance with the SEM observations below. As a final result, the CM with 10 wt.% of PVA is the membrane that reaches the highest rejection at 20 ppm (93.83%) and 100 ppm (94.01%) of feed concentration.

3.1.6. SEM observation

The morphological structure of fabricated membranes was observed using SEM. Fig. 7 shows the SEM images

of the Pz/MP support as well as the PmPD/PVA membranes with different percentages of PVA ranging from 8 to 12 wt.%. As shown in Fig. 7a, the MF support has a microporous structure with a heterogeneous and irregular distribution of particles. This is due to the difference in particle size of materials used in the support preparation (Pozzolan <50 μm and phosphate < 1 μm) [25]. Fig. 7b reveals that the deposited PmPD particles have a spherical shape with a diameter ranging from 300 to 500 nm, which is approximately the same as reported elsewhere [42]. The addition of 8 wt.% PVA does not homogenize the PmPD distribution on the support surface as cracks are still visible. These cracks in the membrane can allow CR dye

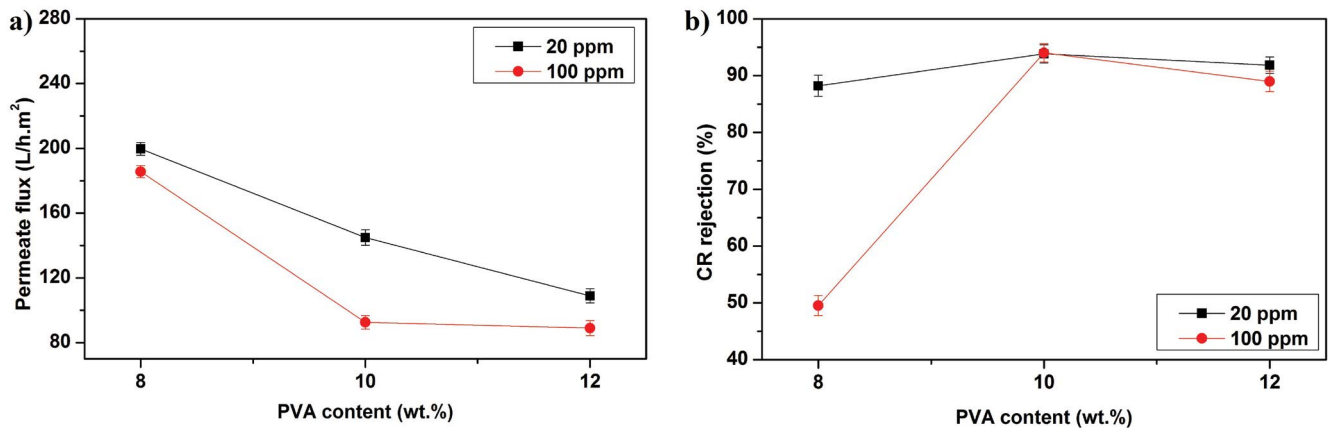


Fig. 6. CR Permeate flux (a) and rejection (b) of CMs with different PVA content at ΔP = 3 bar, C = 20, and 100 ppm for 2 h of filtration.

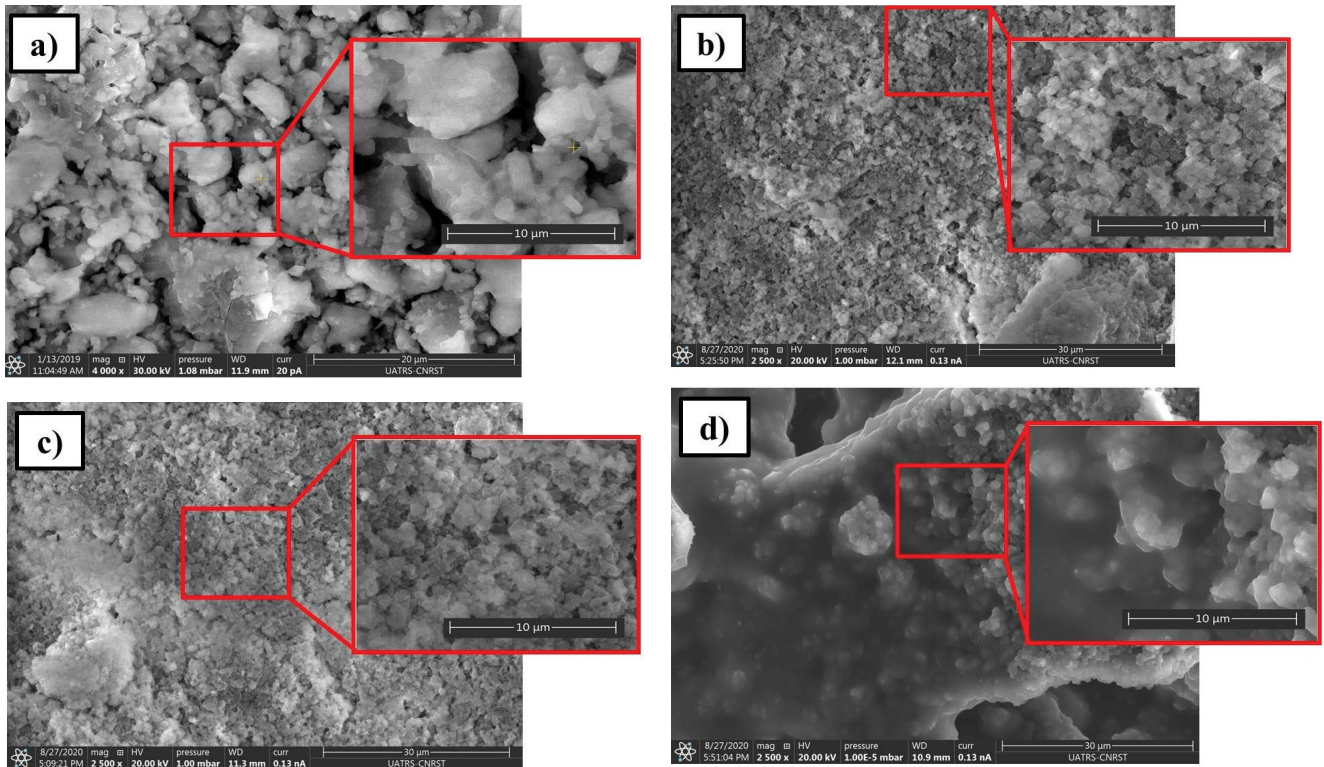


Fig. 7. Top-view SEM micrographs of the Pz/MP support (a), the PmPD/PVA membranes with different PVA content: (b) 8 wt.%, (c) 10 wt.%, and (d) 12 wt.%.

to pass through the CM as described in the previous section. As displayed in Fig. 7c, the membrane with 10 wt.% PVA presents a good deposition of PmPD. The surface of this membrane has a homogeneous morphology and good adhesion. Fig. 7d illustrates that the PmPD membrane with 12 wt.% PVA has a smoother surface [24], with the presence of large, non-uniform pores that will affect the membrane filtration performance.

Fig. 8 shows the cross-section of the three prepared membranes with 8, 10, and 12 wt.% of PVA. It can be seen from these images that increasing the PVA content increases the thickness of the prepared membranes. The thickness of the membrane layer (the average of three measured values for each) is about 14.70 μm for the membrane with 8 wt.% of PVA (Fig. 8a), 19.66 μm for the membrane that contains 10 wt.% of PVA (Fig. 8b) and 22.48 μm for the membrane with 12 wt.% of PVA (Fig. 8c).

From the results of previous sections, as well as SEM images from this section, the highest-performing membrane is the CM with 10 wt.% of PVA and this will be considered as the optimized membrane.

3.1.7. EDX analysis

The chemical composition of the optimized PmPD/PVA membrane was determined by EDX analysis. As shown

in Fig. 9, the intense peaks of carbon (C), oxygen (O), and nitrogen (N) are clearly observed with weight percent of 52.88 wt.%, 31.92 wt.%, and 11.40 wt.%, respectively. It should be noted that the PmPD is a compound of C and N, while the PVA is a compound of C and O. The presence of chlorine (Cl) is attributed to the mPD polymerization by FeCl_3 . The presence of trace amounts of other elements including sulfur (S), sodium (Na), silicon (Si), potassium (K), calcium (Ca), iron (Fe), aluminum (Al) is due to sampling of the chemical composition of the underlying Pz/MP support.

These results indicate that PmPD and PVA contain the expected elemental compositions, consistent with an organic polymer layer deposited on an inorganic, Pz/MP support.

3.2. UF experiments

The PmPD/PVA membrane performance was assessed by the removal efficiency of CR dye. In this part the effect of operating pressure, feed concentration, and pH were investigated for the optimized UF membrane.

3.2.1. Effect of operating pressure

The UF experiments were carried out at operating pressure varying from 1 to 3 bar, a feed concentration of 20 ppm, and a feed pH of 6 which is around the value

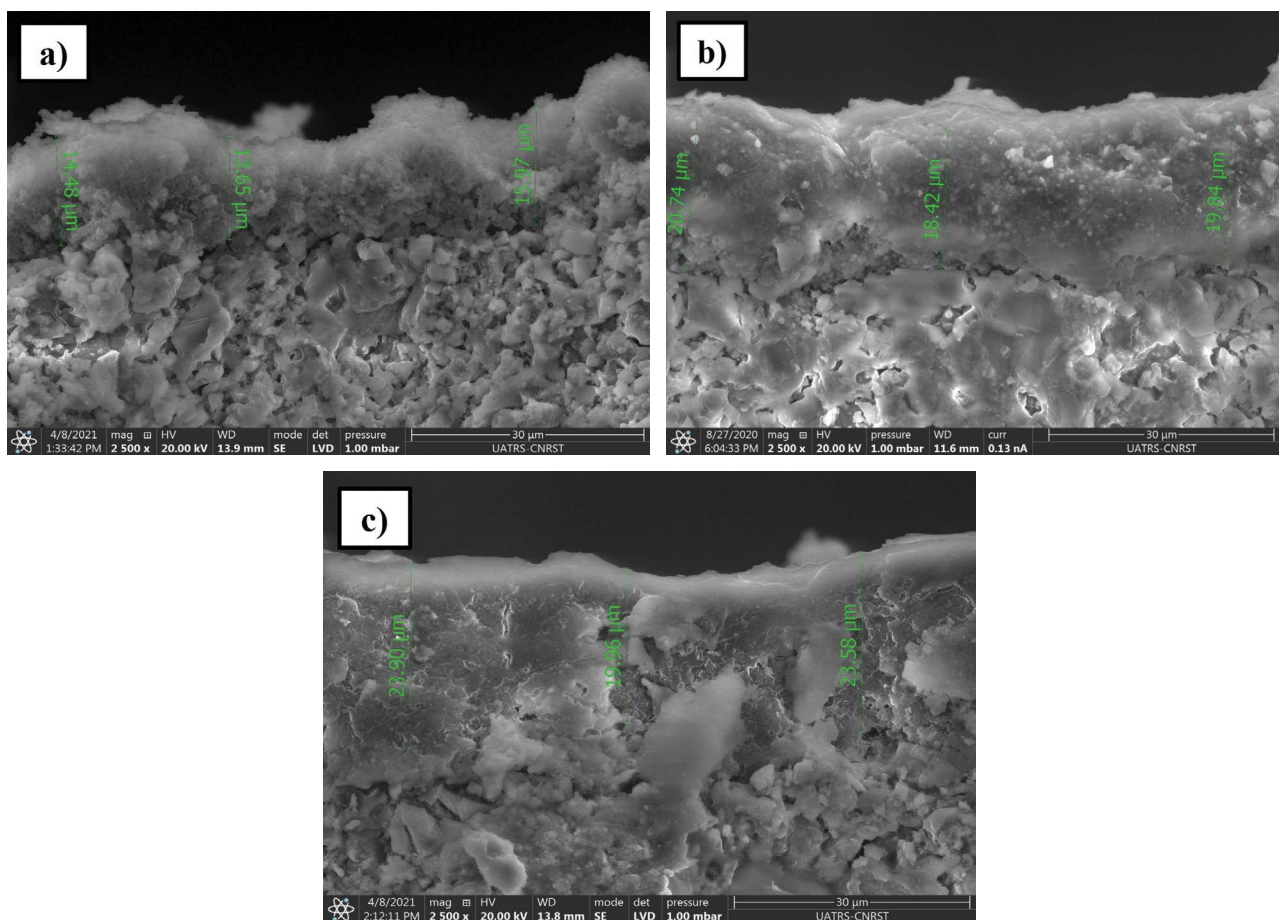


Fig. 8. Cross-section of the membranes with different PVA content: (a) 8 wt.%, (b) 10 wt.%, and (c) 12 wt.%.

of pH_{PZC} calculated of the membrane ($pH_{PZC} = 6.10$). The variation of permeate flux and CR rejection vs. operating pressure are respectively plotted in Fig. 10a and b. When the operating pressure increases (from 1 to 3 bar) the permeate flux after 2 h of filtration also increases from 94.02 to 144.91 L/h m² (Fig. 10a), resulting from the increase of driving force across the membrane [22]. The permeate flux increases with pressure until 2.5 bar where it tends to stabilize. This behavior is due to concentration polarization at the membrane surface. Note that the permeate flux remains lower than the water flux. This may be due to various aspects such as adsorption of CR particles on the surface of the CM and in pores [47].

While increasing the operating pressure (Fig. 10b), the CR rejection after 2 h of filtration increases from 79.20% to 93.83%. This higher rejection qualitatively agrees with the classical (Spiegler–Kedem) convection/diffusion model for solute transport, which predicts that solute rejection by a

partially retentive membrane should increase with operating solvent flux [48].

3.2.2. Effect of feed concentration

The effect of CR feed concentration (20–600 ppm) on the permeate flux and rejection was investigated at a constant pressure of 3 bar and a pH of 6 ($pH = pH_{PZC}$) (Fig. 11).

In general, a high feed concentration yields a very low permeate flux [48]. As expected, the permeate flux decreases from 144.91 to 17.92 L/h m² when the feed concentration increases from 20 to 600 ppm (Fig. 11a). This trend might be related to the anionic CR particles that have settled either on the membrane surface or into the pores thus raising membrane fouling and resulting in a reduction in permeate flux. Also, an increase in concentration polarization might be responsible for this observation [47] as well as the adsorption of the dye on the membrane surface [49].

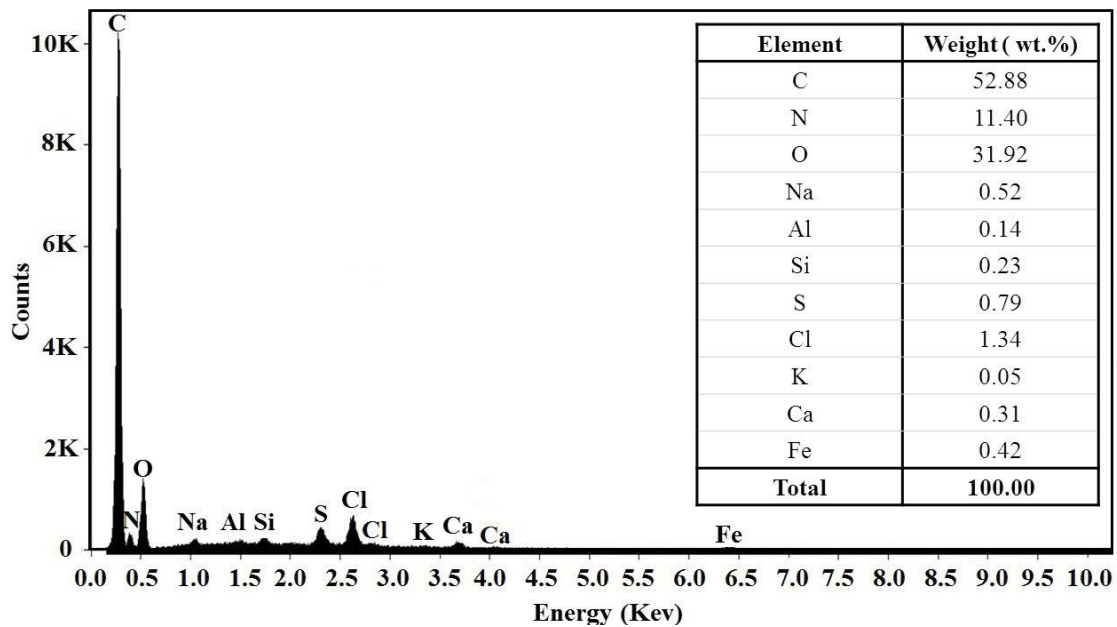


Fig. 9. EDX spectrum of PmPD/PVA membrane.

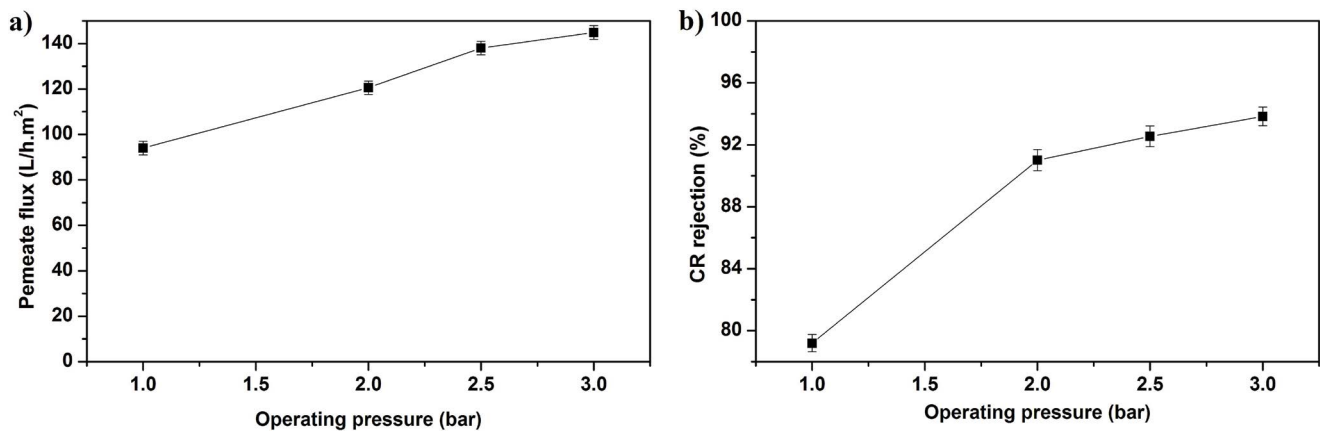


Fig. 10. CR permeate flux (a) and rejection (b) as a function of operating pressure at C = 20 ppm and pH = 6 for 2 h of filtration.

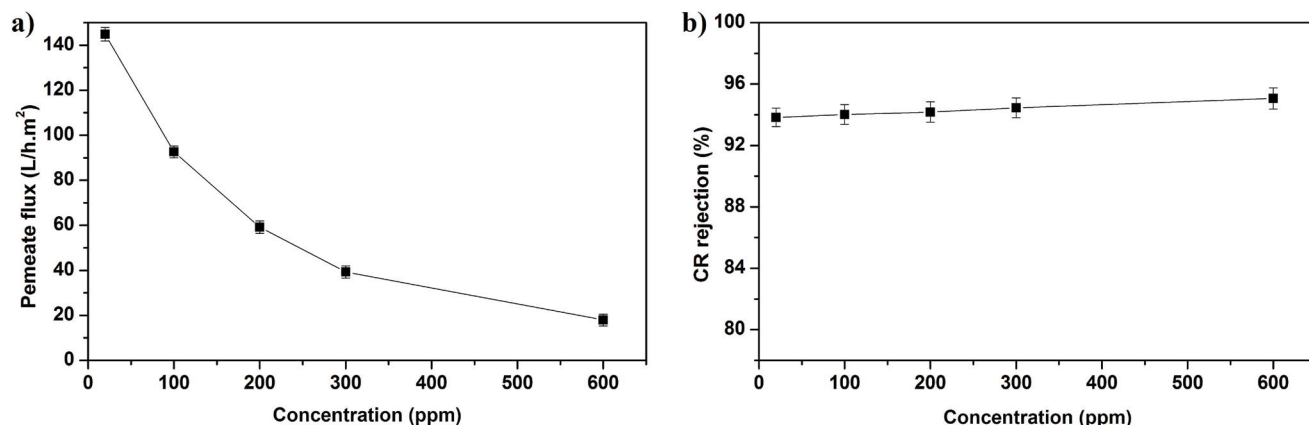


Fig. 11. CR permeate flux (a) and rejection (b) as a function of feed concentration at $\Delta P = 3$ bar and $pH = 6$ for 2 h of filtration.

In contrast, the rejection of dye after 2 h of filtration slightly increases with the increase of the feed concentration (Fig. 11b). At 20 ppm the rejection was 93.83% and reached 95.06% when the dye concentration is 600 ppm. The rejection remained relatively constant even as the dye concentration was varied from 20 to 600 ppm which indicates that whatever the concentration is, the rejection of the dye is always important. The same observation was reported in other work [22,47].

These rejection values could be mainly due to the formation of a polarization layer on the membrane surface that acts like a second separating layer during filtration [49]. This means that the only transport mode within this layer is diffusion [50], consistent with conclusions made in other studies [51,52]. In addition, the two negatively-charged sulfonate groups of the CR dye lead to the formation of aggregates or clusters with multiple charges and consequently causes an increase in the effective size of the dye. This, subsequently, creates an electrostatic repulsion effect and can be partially responsible for the enhancement of dye rejection [53–56].

3.2.3. Effect of feed pH

The effect of pH plays an important role during CR removal by UF since it influences both the charge of the dye molecules and the characteristics of the CM [57]. The efficiency of the PmPD/PVA membrane for CR removal in terms of flux and rejection was studied in a pH range of 4–10 under a fixed concentration (600 ppm) and operating pressure (3 bar). Fig. 12 shows that the permeate flux increases (from 14.60 to 23.01 L/h m²) whereas the rejection decreases (from 98.63% to 89.33%) when the pH is varied from 4 to 10. The lowest permeate flux and the highest CR rejection were achieved at the lowest pH value where sediments of dye occur and its color in solution becomes dark blue [58]. Under these acidic conditions, the sulfonated acid groups of CR are protonated, resulting in dye aggregation and precipitation [59]. Thus, the permeate flux decreases because of membrane fouling. This may be due to the aggregation and adsorption of CR within the membrane, blocking the membrane pores [57]. In addition, the weak hydrophilic character of the membrane contributes to fouling as an increase in membrane hydrophilicity reduces fouling phenomena [23].

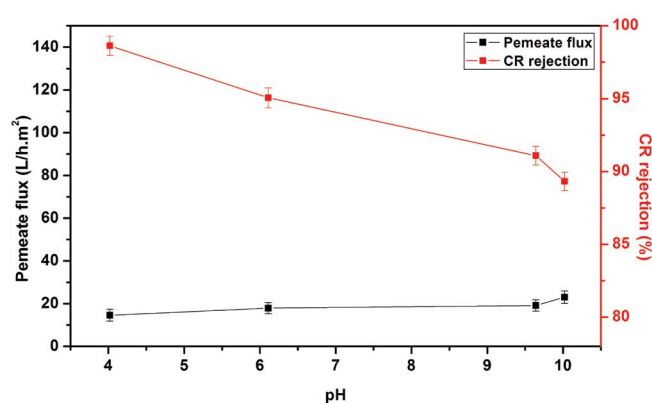


Fig. 12. CR permeate flux and rejection as a function of feed pH at $\Delta P = 3$ bar and $C = 600$ ppm for 2 h of filtration.

The high CR rejection in this acidic medium (98.63%) can also be attributed to the polarization of the surface. The point of zero charges of PmPD/PVA is 6.10 which means that the membrane surface is positively charged under a pH_{PZC} of 6.10 and negatively charged above this pH_{PZC} value. The negatively charged ions of CR would be drawn to the membrane surface by electrostatic attraction, thus creating the polarization layer [22]. This provides repulsion between the surface layer of CR particles and those still in solution as they are both negatively charged. Under basic conditions, at high pH, the permeate flux increases slightly but the rejection decreases. Apparently, the electrostatic attractions became weaker between CR molecules and the membrane surface thus reducing the CR rejection rate [22].

3.3. Antifouling study

During filtration, all membranes gradually become less effective at separating components from the feed solutions. This fouling is coupled with an observable deterioration of the membrane surface. Hence, the CM filtration performance and long-term stability depend greatly on membrane antifouling properties [17,58].

The antifouling study for the PmPD/PVA membrane used for CR removal was evaluated by determining four fouling parameters: FRR, TFR, RFR, and IFR. In order to

facilitate the comparison, all permeate fluxes are normalized to the initial water flux J_{w0} .

Fig. 13a illustrates the water permeate flux before and after filtration, and the permeate flux of CR whereas Fig. 13b shows the antifouling indexes FRR, TFR, RFR, and IFR. The permeate flux of the CM before cleaning (pH = 10 and C = 600 ppm) is less than the permeate flux of water due to the combination of pore-blocking and the formation of a polarization layer on the membrane surface as well as the adsorption of CR dye on the membrane surface. Despite that, a significant restoration in the rate of water permeates flux was observed after physical cleaning with water. From Fig. 13b, it is remarkable that the permeate flux recovers to 34.16% (FRR). Regarding the TFR, it has a value of 96.16% which could be explained by the blockage of pores, surface adsorption as well as a formation of a concentrated polarization layer on the membrane surface. The fouling resulting from the polarization layer surface

can be measured by calculating the RFR (30.33%) and can be removed easily by simple washing. However, the pore blockage is irreversible and can be quantified by measurement of IFR (65.83%) and cannot be removed even by strong force but only by chemical cleaning [60].

3.4. Comparison of composite PmPD/PVA performance with the literature

To compare the efficiency of the current composite PmPD/PVA membrane in water permeability and dye rejection, results of other CMs developed from different organic/inorganic materials reported in the literature for dye rejection are given in Table 3.

According to the presented data, the PmPD/PVA membrane has the highest water permeability compared to all other composite membranes except that of Ppy-PAN-H [61] that has the same value. Whereas the PmPD/

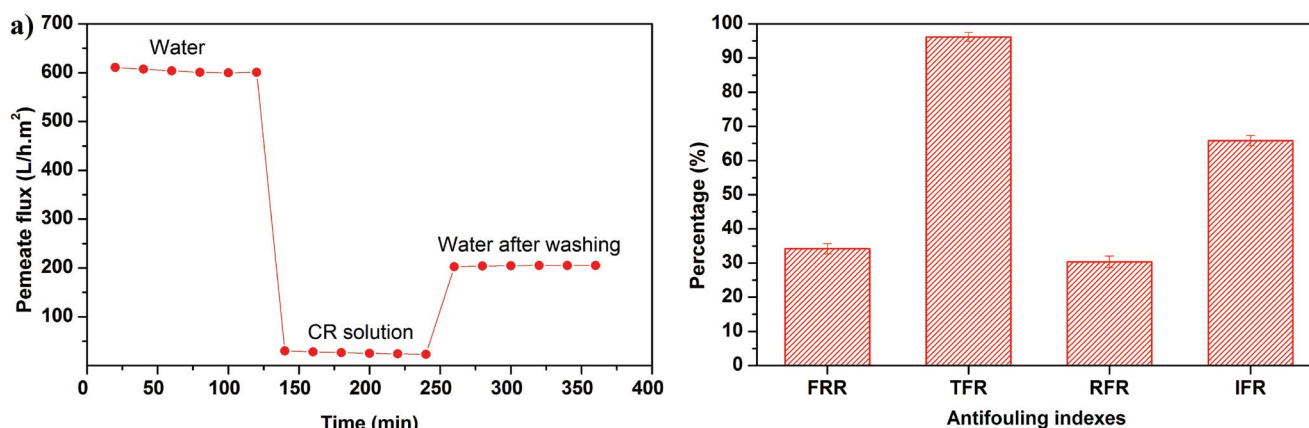


Fig. 13. Permeate flux during filtration experiments (a) and antifouling indexes of PmPD/PVA membrane (b).

Table 3

Comparative study of CM membrane performances with other membranes from literature

| ^a Composite membrane (layer – support) | Pressure (bar) | Permeate flux (L/h m ²) | Permeability (L/h m ² bar) | ^b Dye | Concentration dye (ppm) | Rejection (%) | Ref. |
|---|----------------|-------------------------------------|---------------------------------------|------------------|-------------------------|---------------|-----------|
| Ppy – pozzolan | 3 | 30.90 | 10.30 | CR | 600 | 98.00 | [22] |
| PSF/PEI – pozzolan | 3 | 72.60 | 24.20 | MO | 50 | 75.80 | [23] |
| PVA/ZnO – PSF | 1 | – | – | CR | 100 | 53.50 | [31] |
| PI-Polyester | 1 | 345.10 | 345.10 | CR | 100 | 95.00 | [59] |
| Caramel – PSF | 1 | 355.00 | 355.00 | CR | 50 | 99.94 | [60] |
| Ppy – PAN-H | 4 | 872.00 | 218.00 | RB | 68 | 87.00 | [61] |
| SMWCNT/PES | 6 | 79.40 | 13.23 | CR | 1,000 | 99.80 | [62] |
| 2D MXene – PES | 1 | 115.00 | 115.00 | CR | 100 | 92.30 | [63] |
| PVA-Zeolite | 5 | 3.54 | 0.70 | MB | 1,000 | 93.50 | [64] |
| GA/PVA/PAA-Al ₂ O ₃ | 6 | 25.24 | 4.20 | CR | 100 | 96.00 | [65] |
| PmPD/PVA – pozzolan/ micronized phosphate | 3 | 610.98 | 203.66 | CR | 600 | 98.63 | This work |

^aPpy: Polypyrrole; PSF: Polysulfone; PEI: Polyetherimide; PVA: Poly(vinyl alcohol); PI: Polyimide; PAN-H: Hydrolyzed poly (acrylonitrile); SMWCNT: Sulfonated multiwall carbon nanotubes; 2D MXene: new 2D transition metal carbide-based material; PES: Polyethersulfone; GA: glutaraldehyde; PAA: Poly(acrylic acid); PmPD: poly(m-phenylenediamine).

^bCR: Congo red; MO: Methyl orange; RB: Rose bengal; MB: Methylene blue.

PVA membrane shows higher efficiency of dye rejection compared to the PSF/PEI – pozzolan [23] and PSF/PVA/ZnO [31] membranes, and similar dye rejection for Ppy – pozzolan [22], SMCNT/PES [62], and PSF – caramel [60] membranes. Considering these performance metrics (water permeability and rejection) and the simplicity of preparation, the PmPD/PVA membrane is very competitive for anionic dye rejection from water and could be used for dye wastewater treatment.

4. Conclusion

A composite PmPD/PVA membrane was successfully prepared on a Pz/MP support by dip-coating. Evaluation of the effect of PVA content on UF membrane performance led to an optimized membrane containing 10 wt.% of PVA with the combined highest CR rejection and permeability. FTIR confirmed the formation of PmPD and the co-deposited membrane layer (PmPD/PVA). SEM images showed that the PmPD/PVA layer had a homogeneous surface, uniform thickness (19.67 μm), a pore size of 71 nm, and good adherence to the Pz/MP support. The water permeability of the CM is about 203.66 L/h m^2 bar and the WCA had a value of 80°.

The optimized conditions for CR removal in terms of operating pressure, feed concentration, and feed pH were determined. The rejection reached 98.63% at 600 ppm of CR in an acidic medium (pH = 4) under an operating pressure of 3 bar. In addition, the membrane exhibits attractive anti-fouling characteristics. Based on these promising results, the elaborated CM presented in this paper could be effective for removing soluble dyes from industrial wastewater typically generated by textile industries.

Acknowledgments

This work was supported by MESRSFC (Ministère de l'Enseignement Supérieur et de la Recherche Scientifique et de la Formation des cadres – Morocco). The authors thank UARIS (Unité d'Appui Technique à la Recherche Scientifique) Rabat – Morocco for physicochemical analyses. JC gratefully acknowledges the Lake Forest College sabbatical program and support from the J. William Fulbright Foreign Scholarship Board.

References

- [1] M. Amarine, B. Lekhlif, M. Sinan, A.E. Rharras, J. Echaabi, Treatment of nitrate-rich groundwater using electrocoagulation with aluminum anodes, *Groundwater Sustainable Dev.*, 11 (2020) 1–11.
- [2] N. Nabbou, M. Belhachemi, M. Boumelik, T. Merzougui, D. Lahcene, Y. Harek, A.A. Zorpas, M. Jeguirim, Removal of fluoride from groundwater using natural clay (kaolinite): optimization of adsorption conditions, *C.R. Chim.*, 22 (2019) 105–112.
- [3] J. Cuhorka, E. Wallace, P. Mikulášek, Removal of micropollutants from water by commercially available nanofiltration membranes, *Sci. Total Environ.*, 720 (2020) 1–11.
- [4] J.S. Ra, T.Y. Jeong, S.H. Lee, S.D. Kim, Application of toxicity identification evaluation procedure to toxic industrial effluent in South Korea, *Chemosphere*, 143 (2016) 71–77.
- [5] P. Banerjee, T.K. Dey, S. Sarkar, S. Swarnakar, A. Mukhopadhyay, S. Ghosh, Treatment of cosmetic effluent in different configurations of ceramic UF membrane based bioreactor: toxicity evaluation of the untreated and treated wastewater using catfish (*Heteropneustes fossilis*), *Chemosphere*, 146 (2016) 133–144.
- [6] P. Sharma, S. Tripathi, N. Vadakedath, R. Chandra, *In-situ* toxicity assessment of pulp and paper industry wastewater on *Trigonella foenum-graecum* L: potential source of cytotoxicity and chromosomal damage, *Environ. Technol. Innovation*, 21 (2020) 1–16.
- [7] A.K. Verma, Treatment of textile wastewaters by electrocoagulation employing Fe-Al composite electrode, *J. Water Process Eng.*, 20 (2017) 168–172.
- [8] E.A. Khan, Shahjahan, T.A. Khan, Adsorption of methyl red on activated carbon derived from custard apple (*Annona squamosa*) fruit shell: equilibrium isotherm and kinetic studies, *J. Mol. Liq.*, 249 (2018) 1195–1211.
- [9] M.M. Dantie, Y.C. Woo, B. Kim, R.H. Hailemariam, K.D. Park, H.K. Shon, C. Park, J.S. Choi, Removal of fluoride in membrane-based water and wastewater treatment technologies: performance review, *J. Environ. Manage.*, 251 (2019) 1–24.
- [10] N. Boudechiche, M. Fares, S. Ouyahia, H. Yazid, M. Trari, Z. Sadaoui, Comparative study on removal of two basic dyes in aqueous medium by adsorption using activated carbon from *Ziziphus lotus* stones, *Microchem. J.*, 146 (2019) 1010–1018.
- [11] G. Derouich, S.A. Younsi, J. Bennazha, B. Achiou, M. Ouammou, I.E.A.E. Hassani, A. Albizane, Adsorption study of cationic and anionic dyes onto Moroccan natural pozzolan. Application for removal of textile dyes from aqueous solutions, *Desal. Water Treat.*, 145 (2019) 348–360.
- [12] M.S. Anantha, S. Olivera, C. Hu, B.K. Jayanna, N. Reddy, K. Venkatesh, H.B. Muralidhara, R. Naidu, Comparison of the photocatalytic, adsorption and electrochemical methods for the removal of cationic dyes from aqueous solutions, *Environ. Technol. Innovation*, 17 (2020) 1–20.
- [13] L.G.M. Silva, F.C. Moreira, M.A.P. Cechinel, L.P. Mazur, A.A.U.D. Souza, S.M.A.G.U. Souza, R.A.R. Boaventura, V.J.P. Vilar, Integration of Fenton's reaction based processes and cation exchange processes in textile wastewater treatment as a strategy for water reuse, *J. Environ. Manage.*, 272 (2020) 1–14.
- [14] A. Mortadi, E.G. Chahid, A. Elmelouky, M. Chahbi, N.E. Ghyati, S. Zaim, O. Cherkaoui, R.E. Moznine, Complex electrical conductivity as a new technique to monitor the coagulation-flocculation processes in the wastewater treatment of the textile industry, *Water Resour. Ind.*, 24 (2020) 1–6.
- [15] E. Alver, M. Bulut, A.Ü. Metin, H. Çiftçi, One step effective removal of Congo Red in chitosan nanoparticles by encapsulation, *Spectrochim. Acta, Part A*, 171 (2017) 132–138.
- [16] M. Tian, R. Wang, A. Goto, W. Mao, Y. Miyoshi, H. Mizoguchi, Performance enhancement of ultrafiltration membrane via simple deposition of polymer-based modifiers, *J. Water Process Eng.*, 33 (2020) 1–7.
- [17] H. Ouaddari, A. Karim, B. Achiou, S. Saja, A. Aaddane, J. Bennazha, I.E.A.E. Hassani, M. Ouammou, A. Albizane, New low-cost ultrafiltration membrane made from purified natural clays for direct Red 80 dye removal, *J. Environ. Chem. Eng.*, 7 (2019) 1–10.
- [18] S. Mestre, A. Gozalbo, M.M.L. Ayza, E. Sánchez, Low-cost ceramic membranes: a research opportunity for industrial application, *J. Eur. Ceram. Soc.*, 39 (2019) 3392–3407.
- [19] F.M. Sukma, P.Z.Ç. Emecen, Cellulose membranes for organic solvent nanofiltration, *J. Membr. Sci.*, 545 (2018) 329–336.
- [20] M. Ji, J. Luo, J. Wei, J. Woodley, A.E. Daugaard, M. Pinelo, Commercial polysulfone membranes pretreated with ethanol and NaOH: effects on permeability, selectivity and antifouling properties, *Sep. Purif. Technol.*, 219 (2019) 82–89.
- [21] Y. Zhang, Y. Wan, G. Pan, X. Wei, Y. Li, H. Shi, Y. Liu, Preparation of high performance polyamide membrane by surface modification method for desalination, *J. Membr. Sci.*, 573 (2019) 11–20.
- [22] G. Derouich, S. Alami Younsi, J. Bennazha, J.A. Cody, M. Ouammou, M.E. Rhazi, Development of low-cost polypyrrole/sintered pozzolan ultrafiltration membrane and its highly efficient performance for congo red dye removal, *J. Environ. Chem. Eng.*, 8 (2020) 1–10.

- [23] S. Benkhaya, B. Achiou, M. Ouammou, J. Bennazha, S.A. Younssi, S. M'rabet, A.E. Harfi, Preparation of low-cost composite membrane made of polysulfone/polyetherimide ultrafiltration layer and ceramic pozzolan support for dyes removal, *Mater. Today Commun.*, 19 (2019) 212–219.
- [24] M. Samei, T. Mohammadi, A.A. Asadi, Tubular composite PVA ceramic supported membrane for bio-ethanol production, *Chem. Eng. Res. Des.*, 91 (2013) 2703–2712.
- [25] D. Beqqour, B. Achiou, A. Bouazizi, H. Ouaddari, H. Elomari, M. Ouammou, J. Bennazha, S. Alami Younssi, Enhancement of microfiltration performances of pozzolan membrane by incorporation of micronized phosphate and its application for industrial wastewater treatment, *J. Environ. Chem. Eng.*, 7 (2019) 1–10.
- [26] Y. Chen, S. Xu, S. Han, S. Chu, L. Yang, C. Jiang, Reusable and removable PmPD/PVA membrane for effective Cr(VI) adsorption and reduction, *New J. Chem.*, 43 (2019) 5039–5046.
- [27] M.R. Huang, Q.Y. Peng, X.G. Li, Rapid and effective adsorption of lead ions on fine poly(phenylenediamine) microparticles, *Chem. Eur. J.*, 12 (2006) 4341–4350.
- [28] A.A. Sapalidis, Porous polyvinyl alcohol membranes: preparation methods and applications, *Symmetry*, 12 (2020) 1–22.
- [29] M. Dmitrenko, A. Penkova, A. Kuzminova, A. Missyul, S. Ermakov, D. Roizard, Development and characterization of new pervaporation PVA membranes for the dehydration using bulk and surface modifications, *Polymers*, 10 (2018) 1–20.
- [30] N.A.M. Nazri, W.J. Lau, A.F. Ismail, T. Matsuura, D. Veerasamy, N. Hilal, Performance of PAN-based membranes with graft copolymers bearing hydrophilic PVA and PAN segments in direct ultrafiltration of natural rubber effluent, *Desalination*, 358 (2015) 49–60.
- [31] N.P. Khumalo, G.D. Vilakati, S.D. Mhlanga, A.T. Kuvarega, B.B. Mamba, J. Li, D.S. Dlamini, Dual-functional ultrafiltration nano-enabled PSf/PVA membrane for the removal of Congo red dye, *J. Water Process Eng.*, 31 (2019) 1–8.
- [32] A. Belgada, B. Achiou, S. Alami Younssi, F.Z. Charik, M. Ouammou, J.A. Cody, R. Benhida, K. Khaless, Low-cost ceramic microfiltration membrane made from natural phosphate for pretreatment of raw seawater for desalination, *J. Eur. Ceram. Soc.*, 41 (2021) 1613–1621.
- [33] R. Mouratib, Low-cost ceramic membrane made from alumina- and silica-rich water treatment sludge and its application to wastewater filtration, *J. Eur. Ceram. Soc.*, 40 (2020) 5942–5950.
- [34] A. Ahmad, M. Rafatullah, O. Sulaiman, M.H. Ibrahim, R. Hashim, Scavenging behaviour of meranti sawdust in the removal of methylene blue from aqueous solution, *J. Hazard. Mater.*, 170 (2009) 357–365.
- [35] I. Amer, D.A. Young, H.C.M. Vosloo, Chemical oxidative polymerization of m-phenylenediamine and its derivatives using aluminium triflate as a co-catalyst, *Eur. Polym. J.*, 49 (2013) 3251–3260.
- [36] Z. Wu, S. Yang, Z. Chen, T. Zhang, T. Guo, Z. Wang, F. Liao, Synthesis of Ag nanoparticles-decorated poly(m-phenylenediamine) hollow spheres and the application for hydrogen peroxide detection, *Electrochim. Acta*, 98 (2013) 104–108.
- [37] W. Yu, L. Zhang, H. Wang, L. Chai, Adsorption of Cr(VI) using synthetic poly(m-phenylenediamine), *J. Hazard. Mater.*, 260 (2013) 789–795.
- [38] L. Zhang, H. Wang, W. Yu, Z. Su, L. Chai, J. Li, Y. Shi, Facile and large-scale synthesis of functional poly(m-phenylenediamine) nanoparticles by Cu²⁺ assisted method with superior ability for dye adsorption, *J. Mater. Chem.*, 22 (2012) 18244–18251.
- [39] L. Zhang, L. Chai, J. Liu, H. Wang, W. Yu, P. Sang, pH manipulation: a facile method for lowering oxidation state and keeping good yield of poly(m-phenylenediamine) and its powerful ag⁺ adsorption ability, *Langmuir*, 27 (2011) 13729–13738.
- [40] A. Xie, L. Ji, S. Luo, Z. Wang, Y. Xu, Y. Kong, Synthesis, characterization of poly(m-phenylenediamine)/palygorskite and its unusual and reactive adsorbability to chromium(VI), *New J. Chem.*, 38 (2014) 777–783.
- [41] L. Jin, L. Chai, L. Ren, Y. Jiang, W. Yang, S. Wang, Q. Liao, H. Wang, L. Zhang, Enhanced adsorption-coupled reduction of hexavalent chromium by 2D poly(m-phenylenediamine)-functionalized reduction graphene oxide, *Environ. Sci. Pollut. Res.*, 26 (2019) 31099–31110.
- [42] L. Xu, J. Ma, N. Zhou, P. Guo, G. Wang, C. Su, Well-dispersed poly(m-phenylenediamine)/silver composite for non-enzymatic amperometric glucose sensor applied in a special alkaline environment, *Ionics*, 24 (2018) 2795–2805.
- [43] E.A.Z. Contreras, C.A.H. Escobar, A.V. Rios, S.G.F. Gallardo, T. Kobayashi, Diaminium salt as reactive amphiphile for the synthesis of poly(m-phenylenediamine) and paraffin microencapsulation, *Colloid Polym. Sci.*, 293 (2015) 2635–2645.
- [44] X.G. Li, M.R. Huang, T. Tao, Z. Ren, J. Zeng, J. Yu, T. Umeyama, T. Ohara, H. Imahori, Highly cost-efficient sorption and desorption of mercury ions onto regenerable poly(m-phenylenediamine) microspheres with many active groups, *Chem. Eng. J.*, 391 (2020) 123515, doi: 10.1016/j.cej.2019.123515.
- [45] A. Kharazmi, N. Faraji, R.M. Hussin, E. Saion, W.M.M. Yunus, K. Behzad, Structural, optical, opto-thermal and thermal properties of ZnS-PVA nanofluids synthesized through a radiolytic approach, *Beilstein J. Nanotechnol.*, 6 (2015) 529–536.
- [46] N.V. Bhat, M.M. Nate, M.B. Kurup, V.A. Bambole, S. Sabharwal, Effect of γ -radiation on the structure and morphology of polyvinyl alcohol films, *Nucl. Instrum. Methods Phys. Res., Sect. B*, 237 (2005) 585–592.
- [47] R.V. Kumar, A.K. Ghoshal, G. Pugazhenth, Fabrication of zirconia composite membrane by *in-situ* hydrothermal technique and its application in separation of methyl orange, *Ecotoxicol. Environ. Saf.*, 121 (2015) 73–79.
- [48] Y. He, G. Li, H. Wang, J. Zhao, H. Su, Q. Huang, Effect of operating conditions on separation performance of reactive dye solution with membrane process, *J. Membr. Sci.*, 321 (2008) 183–189.
- [49] A. Bouazizi, M. Breida, A. Karim, B. Achiou, M. Ouammou, J.I. Calvo, A. Aaddane, K. Khiat, S.A. Younssi, Development of a new TiO₂ ultrafiltration membrane on flat ceramic support made from natural bentonite and micronized phosphate and applied for dye removal, *Ceram. Int.*, 43 (2017) 1479–1487.
- [50] S.M.K. Sadr, D.P. Saroj, Membrane technologies for municipal wastewater treatment, *Adv. Membr. Technol. Water Treat.*, (2015) 443–463, doi: 10.1016/B978-1-78242-121-4.00014-9.
- [51] M. Jiang, K. Ye, J. Lin, X. Zhang, W. Ye, S. Zhao, B.V.D. Bruggen, Effective dye purification using tight ceramic ultrafiltration membrane, *J. Membr. Sci.*, 566 (2018) 151–160.
- [52] A. Bouazizi, M. Breida, B. Achiou, M. Ouammou, J.I. Calvo, A. Aaddane, S.A. Younssi, Removal of dyes by a new nano-TiO₂ ultrafiltration membrane deposited on low-cost support prepared from natural Moroccan bentonite, *Appl. Clay Sci.*, 149 (2017) 127–135.
- [53] J. Lin, W. Ye, M.C. Baltaru, Y.P. Tang, N.J. Bernstein, P. Gao, S. Balta, M. Vlad, A. Volodin, A. Sotto, P. Luis, A.L. Zydney, B.V.D. Bruggen, Tight ultrafiltration membranes for enhanced separation of dyes and Na₂SO₄ during textile wastewater treatment, *J. Membr. Sci.*, 514 (2016) 217–228.
- [54] P. Skrabal, F. Bangerter, K. Hamada, T. Iijima, Entropy contribution to an azo dye aggregation in aqueous solution, *Dyes Pigm.*, 8 (1987) 371–374.
- [55] K. Hamada, H. Kubota, A. Ichimura, T. Iijima, S. Amiya, Aggregation of an azo dye in aqueous solution, *Ber. Bunsenges. Phys. Chem.*, 89 (1985) 859–863.
- [56] K. Hamada, H. Nonogaki, Y. Fukushima, B. Munkhbat, M. Mitsuishi, Effects of hydrating water molecules on the aggregation behavior of azo dyes in aqueous solutions, *Dyes Pigm.*, 16 (1991) 111–118.
- [57] N.H.H. Hairom, A.W. Mohammad, A.A.H. Kadhum, Nanofiltration of hazardous Congo red dye: performance and flux decline analysis, *J. Water Process Eng.*, 4 (2014) 99–106.
- [58] C. Liu, H. Mao, J. Zheng, S. Zhang, Tight ultrafiltration membrane: preparation and characterization of thermally resistant carboxylated cardo poly(arylene ether ketone)s (PAEK-COOH) tight ultrafiltration membrane for dye removal, *J. Membr. Sci.*, 530 (2017) 1–10.

- [59] C. Yang, W. Xu, Y. Nan, Y. Wang, Y. Hu, C. Gao, X. Chen, Fabrication and characterization of a high performance polyimide ultrafiltration membrane for dye removal, *J. Colloid Interface Sci.*, 562 (2020) 589–597.
- [60] C. Lavanya, K. Soontarapa, M.S. Jyothi, R.G. Balakrishna, Environmental friendly and cost-effective caramel for congo red removal, high flux, and fouling resistance of polysulfone membranes, *Sep. Purif. Technol.*, 211 (2019) 348–358.
- [61] X. Li, P. Vandezande, I.F.J. Vankelecom, Polypyrrole modified solvent resistant nanofiltration membranes, *J. Membr. Sci.*, 320 (2008) 143–150.
- [62] J. Zheng, M. Li, K. Yu, J. Hu, X. Zhang, L. Wang, Sulfonated multiwall carbon nanotubes assisted thin-film nanocomposite membrane with enhanced water flux and anti-fouling property, *J. Membr. Sci.*, 524 (2017) 344–353.
- [63] R. Han, Preparation of a new 2D MXene/PES composite membrane with excellent hydrophilicity and high flux, *RSC Adv.*, 7 (2017) 56204–56210.
- [64] A. Ma'ruf, M.A.S. Al Fatoni, A.M. Purnawanto, I. Meilani, Utilization of natural zeolite for development of ceramic/polymer composite membrane for ultrafiltration, *Artik. J.*, 19 (2019) 1547–1551.
- [65] L. Wang, N. Wang, G. Zhang, S. Ji, Covalent crosslinked assembly of tubular ceramic-based multilayer nanofiltration membranes for dye desalination, *AIChE J.*, 59 (2013) 3834–3842.